

# Simulating Galaxies and Galaxy Clusters

J. Sommer-Larsen<sup>1,2</sup>

<sup>1</sup>Theoretical Astrophysics Center, Juliane Maries Vej 30, 2100 Copenhagen Ø

<sup>2</sup>Nordita, Blegdamsvej 17, 2100 Copenhagen Ø  
e-mail: jslarsen@tac.dk

**Abstract.** The X-ray luminosities of the hot halo gas around simulated, Milky Way like disk galaxies have been determined, as a function of redshift. The X-ray luminosity increases significantly with redshift, in some cases as much as a factor 30 going from  $z=0$  to 2. Consequently, the optimal detection redshift can be  $\gtrsim 0.5$ . Results of fully cosmological simulations of galaxy groups and clusters, incorporating star formation, chemical evolution with non-instantaneous recycling, metal-dependent radiative cooling, galactic super-winds and thermal conduction are presented. X-ray luminosities at  $z=0$  are somewhat high and central entropies somewhat low compared to observations. This is likely a combined effect of chemical evolution and metal-dependent, radiative cooling. Central ICM abundance profiles are somewhat steep, and the observed level of ICM enrichment can only be reproduced with IMFs more top-heavy than the Salpeter IMF. In agreement with observations it is found that the iron in the ICM is in place already at  $z \sim 1$ . The [Si/Fe] of the ICM decreases with time, and increases slightly with radius at a given time. The cluster galaxies match the observed “red sequence” very well, and the metallicity of cluster galaxies increases with galaxy mass, as observed.

**Key words.** Numerical simulations - Galaxies - Clusters of galaxies

## 1. X-ray emission from the haloes of disk galaxies

Standard models of disk galaxy formation require spiral galaxies to be surrounded by large reservoirs of hot gas, which should be emitting at X-ray wavelengths, and from which gas should still be accreting on to the disk at present (e.g., White & Frenk 1991). The detailed properties of these haloes and their role in the formation and evolution of galactic disks remain largely unknown from an observational viewpoint, as the haloes have so far escaped direct detection. Possible exceptions are NGC891 (Bregman

& Houck 1997; Strickland et al. 2004), NGC 2841 (Benson et al. 2000), and the Milky Way itself (e.g., Sidher et al. 1996; Pietz et al 1998), if neglecting cases where (i) the galactic disks show evidence of being disturbed by tidal interactions, or (ii) the X-ray emission at off-disk distances of a few kpc can be attributed to processes originating in the disk such as feedback from star-bursts.

Toft et al. (2002) extracted disk galaxies from fully cosmological hydrodynamical simulations and determined their present-day halo X-ray luminosities, finding consistency with observational upper limits

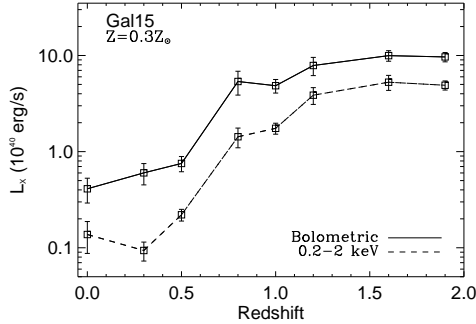


**Fig. 1.** Redshift evolution of the rest-frame bolometric and 0.2–2 keV X-ray luminosities of a simulated, Milky Way like disk galaxy.

on halo emission from nearby spirals. Moreover, based on the predicted rates of mass accretion onto the disks, they suggested that spiral galaxy haloes were possibly one order of magnitude brighter in soft X-rays at  $z \sim 1$  than at present (the gas mass cool-out rate is expected to be proportional to the halo X-ray luminosity times the emissivity weighted inverse temperature of the hot halo gas — see Rasmussen et al. 2004 for details). Analytical models of halo emission overpredict emission at  $z = 0$  by at least an order of magnitude (see Benson et al. 2000 and Toft et al. 2002) and thus cannot be assumed to provide a reliable description of the evolution in X-ray emission with redshift. Rasmussen et al. 2004 extended the work of Toft et al. by studying the higher-redshift properties of two Milky Way like disk galaxies extracted from the  $\Lambda$ CDM galaxy formation simulations of Sommer-Larsen, Götz & Portinari 2003. Figure 1 shows the redshift evolution of the (rest-frame) bolometric and 0.2–2 keV (X-ray) luminosity of the halo of a Milky Way like disk galaxy. The simulation was run with a radiative cooling function corresponding to 1/3 solar abundance. The increase in luminosity is about a factor of 30 going from  $z=0$  to 2. Given this, it is obviously of interest to determine the opti-

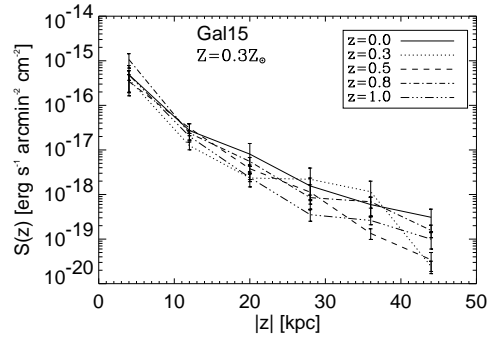


**Fig. 2.** 0.3–2 keV surface brightness of the galaxy from Fig. 1, averaged over 40 kpc wide slabs oriented parallel the disk, as a function of vertical distance  $|z|$  to the disk. The galaxy is viewed edge-on; for each vertical bin, the values above and below the disk have been added.

mal redshift for X-ray halo detection, taking redshifting of the photons, cosmological  $(1+z)^4$  surface brightness dimming, and Galactic HI absorption into account. Rasmussen et al. find that it varies from galaxy to galaxy, but in some cases the optimal detection redshift can be  $\gtrsim 0.5$ . Figure 2 shows for one such case (the galaxy from Fig. 1) the predicted, edge-on 0.3–2 keV surface brightness profiles at various redshifts. An observer at the current epoch would measure the largest surface brightness of this galaxy at  $|z| \lesssim 10$  kpc, when it was at  $z \sim 0.8$ .

## 2. Simulating galaxy groups and clusters — the code and the simulations

Only fairly recently has it been possible to carry out fully cosmological gas-dynamical/N-body simulations of the formation and evolution of galaxy clusters at a level of numerical resolution and physical sophistication that the cool-out of gas, star-formation and chemical evolution in, and outflows from, individual cluster galaxies can be modelled to, at least some, degree

of realism (e.g., Valdarnini 2003; Tornatore et al. 2004).

We have recently engaged in undertaking such simulations of galaxy groups and clusters. Scientific objectives include reproducing the observed luminosity–temperature relation for groups and clusters and its evolution with redshift; surface brightness and entropy profiles; and the high iron abundance of  $\sim 1/3$  solar in the intracluster medium (ICM). The metals have to be first produced in the galaxies and subsequently expelled and mixed into the ICM; since the mass of stars in galaxies is only about 10–20% of the mass of hot ICM gas, this requires high efficiency in metal production and expulsion. Moreover one should reproduce observed ICM abundance profiles and  $\alpha$ –to–iron ratios, “cold fractions”, and group and cluster galaxy luminosity functions and “red sequences”.

The code used for the simulations is a significantly improved version of the TreeSPH code used previously for galaxy formation simulations (Sommer-Larsen, Götz and Portinari 2003): Firstly, we have adopted the “conservative” entropy eq. solving scheme suggested by Springel & Hernquist (2002). Secondly, non-instantaneous chemical evolution tracing 9 elements (He, C, N, O, Mg, Si, S, Ca and Fe) has been incorporated in the code following Lia, Portinari & Carraro (2002). Atomic radiative cooling depending both on the metal abundance of the gas and the meta-galactic UV field is invoked together with simplified radiative transfer. Thirdly, continuing, star-burst and/or AGN driven galactic super-winds are incorporated in the simulations. This is required to get the abundance of the ICM to the observed level of about  $1/3$  solar in iron. The strength of the super-winds is modelled through a free parameter  $f_{\text{wind}}$  which determines how large a fraction of the stars born partake in super-wind driving star formation. We find that in order to get an iron abundance in the ICM comparable to observations,  $f_{\text{wind}} \gtrsim 0.5$  and at the same time a fairly top-heavy Initial Mass Function (IMF) has

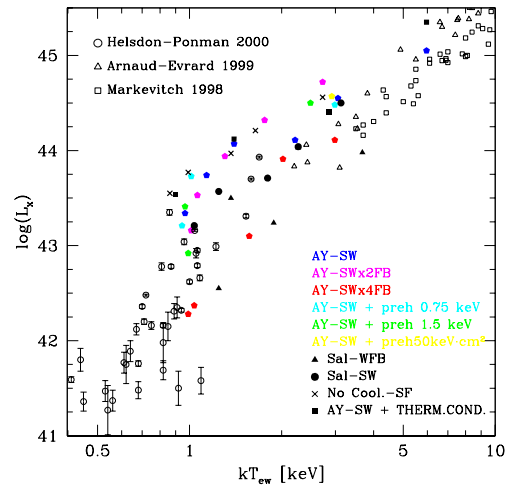


**Fig. 3.**  $L_X - T_X$  relation at  $z=0$ . Data points are marked by open symbols, simulations by filled symbols and crosses. Details about the simulations are given in the text.

to be used — see section 3. Finally, thermal conduction was implemented in the code following Cleary & Monaghan (1999).

Six groups and clusters ( $T=1-6$  keV) were selected from a cosmological,  $L=150 h^{-1}\text{Mpc}$ , “standard”  $\Lambda\text{CDM}$  N-body simulation, and re-simulated with baryonic physics included, using the code described above, for a suite of physical parameters. The wind strength parameter  $f_{\text{wind}}$  was set to 0.7 and Salpeter (Sal) and Arimoto-Yoshii (AY) IMFs were adopted. Some simulations were run with galactic super-wind feedback two times (SWx2FB) and four times (SWx4FB) as energetic as is available from supernovae; the remaining amount of energy is assumed to come from AGN activity. Others were run with an AY IMF, strong feedback (SW) and additional pre-heating at  $z=3$  (AY-SW + preh.), as discussed by Tornatore et al. (2003). One series of simulations was run with a Salpeter IMF and only early ( $z \gtrsim 4$ ), strong feedback, as in the galaxy formation simulations of Sommer-Larsen, Götz and Portinari (2003) (as this results in overall fairly weak feed-

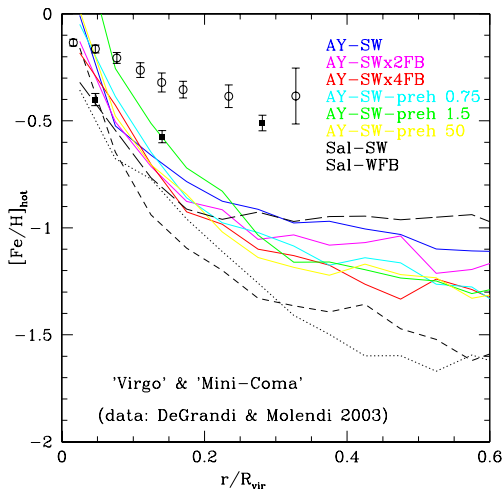


**Fig. 4.** ICM iron abundance profiles for various simulations of the “Virgo” cluster, and one (AY-SW) of the “Mini-Coma” cluster (long-dashed line). Also shown are data points from De Grandi et al. (2003) for cool-core clusters (open circles with errorbars) and non cool-core clusters (filled circles with errorbars). The appropriate comparison of the models is to the cool-core clusters.

back we denote this: Sal-WFB). Another was run with thermal conduction included (AY-SW + Therm.Cond.), assuming a conductivity of 1/3 of the Spitzer value (e.g., Jubelgas et al. 2004). Finally, for comparison with previous work, a series of simulations was run without radiative cooling, star formation and thermal conduction.

### 3. Simulating galaxy groups and clusters — results

In Figure 3 is shown the  $z=0$   $L_X - T$  relation for the 6 groups and clusters ( $T=1-6$  keV), re-simulated with various physical parameters, as explained in the previous section. Also shown are observational data on the  $z=0$   $L_X - T$  relation from various sources. The predicted X-ray luminosities are mostly somewhat high compared to observations, with the exception of models

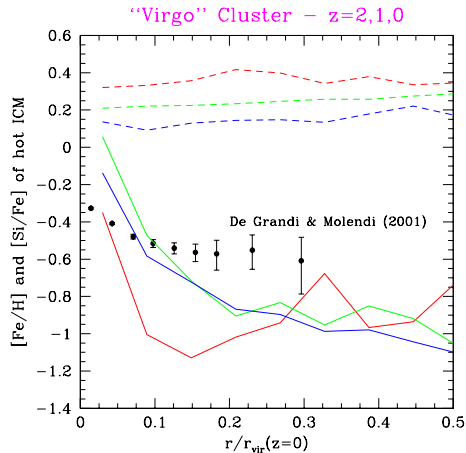


**Fig. 5.** ICM iron abundance profiles for the AY-SW simulation of the “Virgo” cluster at  $z=0, 1$  and  $2$  (solid lines). Also shown are  $[\text{Si}/\text{Fe}]$  profiles at  $z=0, 1$  and  $2$  (dashed lines). To the right  $z=2,1,0$  corresponds to going top down for the two sets of curves ( $z=2$ : red;  $z=1$ : green;  $z=0$ : blue).

run with an Arimoto-Yoshii IMF and very strong feedback (AY-SWx4FB), and models run with a Salpeter IMF and only little feedback (Sal-WFB), hence resulting in a low level of metal enrichment. The preliminary conclusion from the results of these simulations is that the success of previous generations of models in reproducing the  $L_X - T$  relation, the surface brightness profiles, the entropy “floor” at  $S = T/n_e^{2/3} \sim 100-200$  keV cm<sup>2</sup> etc. (e.g., Tornatore et al. 2003) likely was due to the adoption of a primordial radiative cooling function (i.e. the contribution to radiative cooling from metals was neglected). The analysis of this is ongoing, however. For most of our models we find central entropy values of  $\sim 10-20$  keV cm<sup>2</sup>; this may be in agreement with “observed” values in cool-core clusters (M. Voit, this conference).

Figure 4 shows the profiles of iron abundance in the ICM for various models, together with recent observational data by De

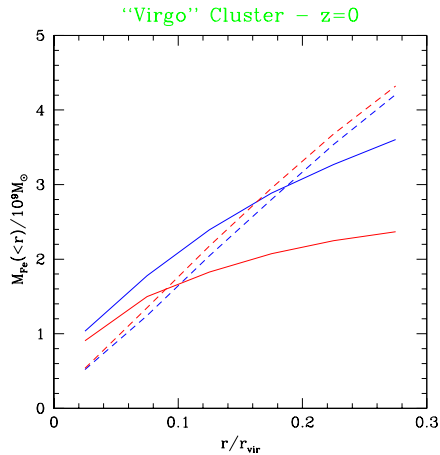


**Fig. 6.** Cumulative iron mass of the ICM at  $z=0$  for the Sal-SW and AY-SW simulations. Actual profiles are shown by solid lines, profiles inferred assuming the observed iron profiles of De Grandi & Molendi (2001) by dashed. Top solid line corresponds to AY-SW, bottom to Sal-SW. Top dashed line corresponds to Sal-SW, bottom to AY-SW (AY: blue; Sal: red).

Grandi et al. (2003). All models, but one, were run for a  $T \simeq 3$  keV cluster, which we shall denote “Virgo” in the following. One model refers to a larger cluster with  $T \simeq 6$  keV, denoted “Mini-Coma”. In general, the iron abundance profiles are too steep in the inner parts of the clusters and too low in the outer parts. In relation to the former problem, AGN induced, buoyant bubbles may help to transport energy and metals from the very central part of clusters outward, flattening the inner abundance profiles. In relation to the latter problem, clear progress is made going from the Salpeter IMF to the more top-heavy Arimoto-Yoshii IMF — see also Portinari et al. 2004. This indicates that an even more top-heavy IMF may be required to reproduce the observed ICM abundance, but see also below.

Figure 5 shows, for the “Virgo” cluster AY-SW simulation, the profiles of  $[\text{Fe}/\text{H}]$

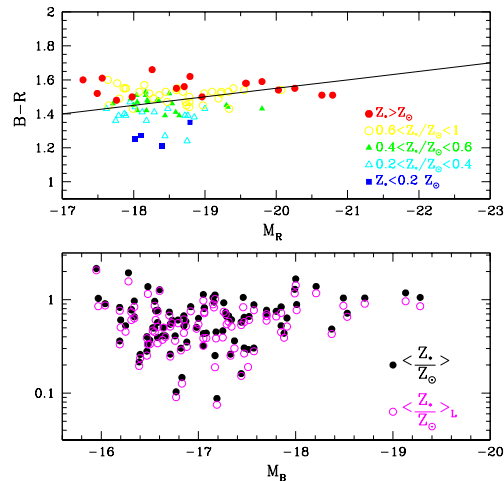


**Fig. 7.** *Top panel:* B-R vs. R Colour-Magnitude relation for the 94 ‘Mini-Coma’ ( $T \sim 6$  keV) cluster galaxies at  $z=0$ , compared to the  $z \simeq 0$  Red Sequence of Gladders et al. (1998) (straight line). *Bottom panel:* Metallicity–luminosity relation for the “Mini-Coma” galaxies (full symbols: mass-weighted, open symbols: luminosity-weighted).

and  $[\text{Si}/\text{Fe}]$  in the ICM, at redshifts  $z=0,1$  and 2. In agreement with observations the metals are essentially in place at  $z=1$  (e.g., Tozzi et al. 2003), and it is seen that substantial enrichment has taken place already at  $z=2$ . This is in agreement with the findings of Sommer-Larsen et al. (2004), that the cluster stars formed at typical redshifts  $z_f \gtrsim 2.5-3$ . Moreover,  $[\text{Si}/\text{Fe}]$  increases slightly with radius at any redshift, also in agreement with observations (Finoguenov et al. 2000). Finally,  $[\text{Si}/\text{Fe}]$  generally decreases with time, as is expected due to the substantial, but delayed iron enrichment of the ICM by supernovae type Ia.

Figure 6 shows the cumulative iron mass in the ICM for the Sal-SW and AY-SW simulations of the “Virgo” cluster. Also shown is the cumulative mass of iron assuming the observed ICM iron profile of De Grandi & Molendi (2001) (similar to the

updated profiles of De Grandi et al. 2003). It is clear that the ICM can not be sufficiently enriched for simulations adopting a Salpeter IMF, whereas this can marginally be accomplished by using an Arimoto-Yoshii IMF (at least out to  $r \sim 0.2-0.3r_{\text{vir}}$ ).

Concerning the properties of the cluster galaxies, shown in Figure 7, at  $z=0$ , is the colour-magnitude (B-R versus R) relation of the 94 galaxies in the “Mini-Coma” cluster (excluding the cD). For comparison is also shown the mean locus of the observed red sequence (solid line) from Gladders et al. (1998). The match to observations is quite satisfactory. Furthermore is shown the mean heavy element abundance for the 94 galaxies versus absolute B-band magnitude. The non-zero slope of the colour-magnitude relation for our cluster galaxies mainly results from the increase of the typical stellar metallicity with galaxy luminosity, as observed (e.g., Kodama & Arimoto 1997).

Full details about our results are given in Romeo, Portinari & Sommer-Larsen (2004), Romeo et al. (2004) and Sommer-Larsen et al. (2004).

### Acknowledgements

I thank the organizers for an excellent conference. We have benefited from discussions with S. Andreon, V. Antonuccio, M. Arnaboldi, S. Borgani, R. Bower, A. Brandenburg, F. Calura, S. De Grandi, K. Freeman, M. Hoeft, D. Kawata, S. Leccia, Y. Lin, F. Matteucci, G. Murante, S. Recchi, L. Tornatore and P. Tozzi.

### References

Benson A. J, Bower R. G., Frenk C. S. & White S.D.M., 2000, MNRAS, 314, 557  
 Bregman J. N. & Houck J. C., 1997, ApJ, 485, 159  
 Cleary P. W. & Monaghan J. J., 1999, Journal of Computational Physics, 148, 227  
 De Grandi S. & Molendi S., 2001, 551, 153  
 De Grandi S., Ettori S., Longhetti M. & Molendi S., 2003, A&A, in press (astro-ph/0310828)

Finoguenov A., David L. P. & Ponman T. J., 2000, ApJ, 544, 188  
 Gladders M. D., Lopez-Cruz O., Yee H. K. C. & Kodama T., 1998, ApJ 501, 571  
 Jubelgas M., Springel V. & Dolag K., 2004, MNRAS, in press (astro-ph/0401456)  
 Kodama T. & Arimoto N., 1997, A&A 320, 41  
 Pietz J., Kerp J., Kalberla P. M. W., Burton W. B., Hartmann D. & Mebold U., 1998, A&A, 332, 55  
 Portinari L., Moretti A., Chiosi C. & Sommer-Larsen J., 2004, ApJ in press (astro-ph/0312360)  
 Rasmussen J., Sommer-Larsen J., Toft S. & Pedersen, K., 2004, MNRAS, 349, 255  
 Romeo A. D., Portinari L. & Sommer-Larsen J., 2004, MNRAS, to be submitted  
 Romeo A.D., Sommer-Larsen J., Portinari L. & Antonuccio V., 2004, in preparation  
 Sidher S. D., Sumner T. J., Quenby J. J. & Gambhir M., 1996, A&A, 305, 308  
 Sommer-Larsen J., Götz, M. & Portinari, L., 2003, ApJ, 596, 47  
 Sommer-Larsen J., Romeo A. D. & Portinari, L., 2004, MNRAS, submitted (astro-ph/0403282)  
 Springel V. & Hernquist L., 2002, MNRAS, 333, 649  
 Strickland D. K., Heckman T. M., Colbert E. J. M., Hoopes C. G. & Weaver K. A., 2004, ApJS, 151, 193  
 Toft S., Rasmussen J., Sommer-Larsen J. & Pedersen K., 2002, MNRAS, 335, 799  
 Tornatore L., Borgani S., Springel V., Matteucci F., Menci N. & Murante G., 2003, MNRAS 342, 1025  
 Tornatore L., Borgani S., Matteucci F., Recchi S. & Tozzi P., 2004, MNRAS in press (astro-ph/0401576)  
 Tozzi P., Rosati P., Ettori S., Borgani S., Mainieri V. & Norman C., 2003, ApJ 593, 705  
 Valdarnini R., 2003, MNRAS 339, 1117  
 White S.D.M. & Frenk C.S., 1991, ApJ, 379, 52